The Thesis committee for Jeffrey Alan Easley, Jr.
Certifies that this is the approved version of the following thesis:

Versatile Chemistry for Designer Polymeric Nanomaterials: Synthesis and Characterization of Self-Assembled Montmorillonite-Block Copolymer Composites

APPROVED BY

SUPERVISING COMMITTEE:

Supervisor: _____

Christopher J. Ellison

_____

C. Grant Willson

Versatile Chemistry for Designer Polymeric Nanomaterials: Synthesis and Characterization of Self-Assembled Montmorillonite-Block Copolymer Composites

by

Jeffrey Alan Easley, Jr., B.S. Ch.Bio.E., B.S. Music

Thesis

Presented to the Faculty of the Graduate School

of the University of Texas at Austin

in Partial Fulfillment

of the Requirements

for the Degree of

Master of Science in Engineering

The University of Texas at Austin

December 2012

Versatile Chemistry for Designer Polymeric Nanomaterials: Synthesis and Characterization of Self-Assembled Montmorillonite-Block Copolymer Composites

by

Jeffrey Alan Easley, Jr., M.S.E.

The University of Texas at Austin, 2012

SUPERVISOR: Christopher J. Ellison

Self-assembled polymer nanocomposites are a promising class of advanced materials with unique structures and tunable properties. Control over the spatial arrangement and ordering of the constituent material is essential to developing composites with defined morphologies and properties. Here I report the synthesis of poly(*n*-butyl acrylate-*b*-styrene) from the surface of functionalized montmorillonite clay (MMT) via activators regenerated by electron transfer (ARGET) atom transfer radical polymerization (ATRP). The application of ARGET ATRP to MMT surface-initiated polymerizations results in a robust and reproducible method for synthesizing well-defined tethered block copolymers. The chosen block copolymer architecture of the composite materials resembles that of a thermoplastic elastomer, with glassy PS domains sandwiching the rubbery PnBA domain, which is divided by the clay platelets. The structure was characterized by several techniques that examine the self-assembly and degree of clay exfoliation. Preliminary analysis of the material properties indicates elastomeric behavior.

Table of Contents

List of Tables

List of Figures

1. Introduction

One of the most studied and revolutionary materials of the 20th century, polymers continue to be ubiquitous in our everyday lives. From use in common household items to the most revolutionary devices, polymers enhance our standard of living and facilitate the development of gadgets previously only imaginable. The rise of polymers in a host of applications, from structural to electronic to biologic, and everything in between, has been enabled notably by advances in polymer composite technology. These composite materials consist of a polymer and filler, ranging from organic to inorganic, of various sizes and geometries. The inclusion of the filler in composite materials enhances the properties over that of the neat matrix polymer, or other advantageous properties of the filler are exploited in unique ways. Researchers continue to develop new types of composites for advanced technological applications.

1.1. Objective

My research herein presented focuses on polymer nanocomposites, in which the filler material has dimensions on the order of several nanometers. Specifically, I have explored synthetic techniques to prepare nanocomposites in which the polymer matrix assists in ordering the filler through surface interactions. The specific nanocomposite I have considered is one in which clay serves as the filler in a block copolymer matrix.

To summarize the primary phases of the research, I first synthesized the block copolymer from an initiator surfactant that ionically binds with the surface of the clay. This feature served to exfoliate individual clay platelets from one another

as the polymer chain grows and to thereby direct the spatial arrangement of the clay in the bulk material. The synthetic method employed is a variant of atom transfer radical polymerization, a controlled polymerization from which block copolymers can be synthesized with known architectures and compositions[1]. The materials were characterized by a variety of morphological and property measurements to ascertain the structure of the material on the nanoscale. Interesting material properties were explored that would be applicable to specific applications, particularly those mechanical in nature.

1.2. Significance

My research has implications for several applications.. The clay nanocomposites are expected to exhibit superior material properties compared to neat polymers, such as strength (modulus), impermeability, and flame retardancy, making them useful for advanced barrier and packaging applications. Additionally, the targeted block copolymer architecture resembles that of thermoplastic elastomers (TPEs), which are both elastic and recyclable, unlike cross-linked, conventional elastic rubbers. The material combines the advantageous features of both commercial TPEs and composite polymeric materials, without requiring the traditional melt processing techniques used to form composites. The inclusion of surface-tethered filler was intended to make this material suitable for high temperature applications where traditional TPEs tend to fail due to increased flow at such temperatures. Many current TPEs are unable to carry filler materials, further limiting their application.

On a broader note, the research indicates that other proposed polymeric nanostructures might be attainable using similar synthetic methods. By altering the filler and chemistry required to attach a suitable initiator moiety, other nanocomposites with controlled architectures may be attainable, such as the idealized structures of hybrid organic solar cells or three dimensional arrays of isolated metallic nanoparticles.

2. Background

An understanding of several areas of polymer research was essential to guide the development of my research. Synthetic methods, the nature of composite polymeric materials, including property enhancement, and the variety of applications for such materials were examined throughout the course of the project.

2.1. Synthetic Methods

In order to synthesize the polymer intended for this research, a controlled polymerization technique was required. It was determined that atom transfer radical polymerization (ATRP) would provide the most direct route to a surface-initiated polymer with a controlled architecture. ATRP was first characterized nearly two decades ago[1-2] and has evolved since then through the extensive investigation of the Matyjaszewski research group. In ATRP, a radical initiator species is activated by a catalyst, typically a transition metal such as copper, which then reacts with a monomer to begin the polymer chain. The radical at the propagating chain end can be activated or deactivated by the catalyst through the addition or subtraction of a halogen atom. When the radical is activated, additional monomer units can react to propagate the chain. At any instant, a majority of the chain ends are deactivated or capped with a halogen atom, reducing the likelihood of coupling or other termination events. This feature of ATRP allows it to be considered a controlled polymerization, in which polymers of predetermined molecular weights (MWs) with low polydispersity can be produced. Additionally, the "living" nature of the propagating radical allows for block copolymers to be easily prepared by the addition of a second monomer[3] or the addition of other end

group functionalities. Nearly any vinyl monomer can by polymerized by ATRP. Unlike other controlled polymerizations, such as anionic, ATRP has relatively low purity requirements and can be conducted without special synthesis equipment[4].

Initial attempts to synthesize the proposed polymeric material proved unsuccessful with conventional ATRP. A different variant of ATRP, activators regenerated by electron transfer (ARGET) ATRP, was ultimately successful. ARGET ATRP requires significantly less catalyst than in typical ATRP because a reducing agent is added that continuously converts the catalyst back to the active state to sustain the propagation reaction[5]. More advanced ligands are required, however, to maintain solubility of the catalytic species[6]. An additional advantage of ARGET ATRP over ATRP is improved control of end group functionality, meaning fewer chains experience termination events, which is especially favorable for block copolymer synthesis[7]. ARGET ATRP also has a relatively high tolerance for impurities and can even be conducted in air, which would typically deactivate the catalyst irreversibly in ATRP[8]. For all these reasons, this variant of ATRP is seen as a viable method for commercial production of polymers with controlled structures.

2.2. Polymer Composites and Property Enhancement

Polymer composites have traditionally been prepared by mixing the filler with a pre-synthesized polymer, usually through melt or solution processing[9]. The degree to which the polymer and filler mixes, particularly how well the filler exfoliates within the polymer matrix, is influenced by processing conditions and the compatibility of the polymer with the surface of the filler. Surfactants may aid in the mixing process. One other approach to enhance exfoliation of clays in composites is

the use of *in situ* polymerization, somewhat similar to the approach outlined here[10]. Materials prepared via this method, however, lack a controlled polymer architecture. My approach to preparing polymer composites specifically addresses limitations with traditional composite preparation.

With regard to properties, polymer composites with assorted fillers exhibit enhanced properties as compared to bulk polymers and are currently employed as alternatives to traditional materials in applications such as reinforcement and barrier membranes[9, 11]. Clay composites, however, lack control over the spatial arrangement and ordering of the constituent material. The spatial arrangement "is as important, if not more so, than simply the degree of refinement of the morphology or the role of the interface region on polymer conformation and dynamics"[12]. For example, studies have shown that barrier properties are significantly enhanced when clays are aligned normal to the direction of diffusion[13] and that the tensile modulus of materials with fully aligned clays increases by 50% when compared to that for materials with random orientations[14].

Block copolymer (BCP) phase behavior is well understood and may be exploited as a directing template for filler materials[15]. Additionally, the filler itself may influence BCP self-assembly. Recent developments in BCP composites have been directed at applications for separation and catalytic membranes[16], optical devices[17], high-density storage[18], and organic electronics[19].

2.3. Proposed Material and Applications

The chosen BCP architecture mimics that of a triblock TPE, with glassy domains sandwiching a rubbery domain, which is divided by the clay platelets. Self-

assembly of the block copolymer directs ordering of the montmorillonite (MMT) in the bulk material. A “macromolecule” of a single clay platelet surrounded by a BCP halo is pictured in Figure 1. The glassy polystyrene block should entangle with that of adjacent “macromolecules” to provide tear resistance and strength in the bulk material. The rubbery poly(*n*-butyl acrylate) block imparts elastic behavior, and the clay provides reinforcement and other potential properties.

Previous efforts to synthesize surface-tethered homopolymers and block copolymers from MMT have been based on anionic polymerization[20] and standard ATRP[21]. These methods, however, have resulted in free polymer in solution because of excess free initiator moieties in solution, which compete with tethered initiators for monomers, resulting in unpredictable molecular weights. The application of ARGET ATRP to MMT surface-initiated polymerizations results in a robust and reproducible method for synthesizing well-defined tethered BCPs.

3. Results and Discussion

3.1. Synthesis of Composite and Non-Composite BCPs

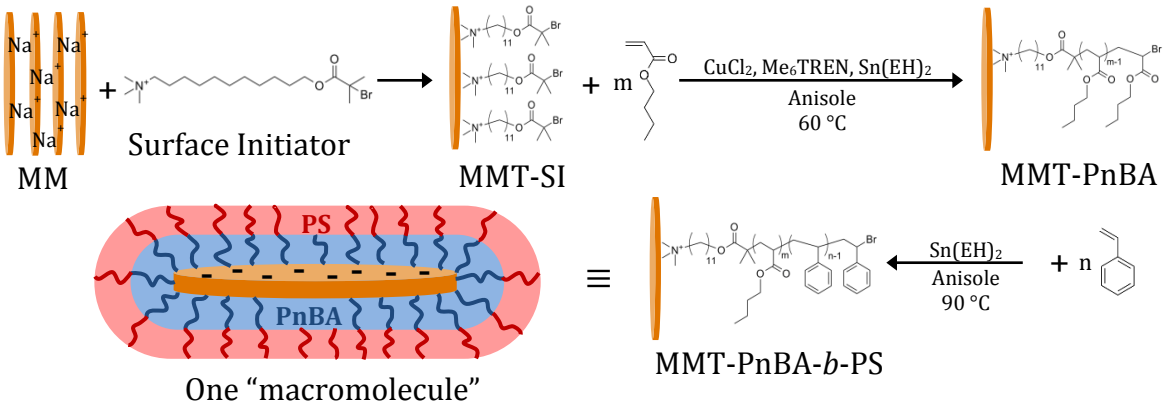

Figure 1. ARGET ATRP of PnBA-*b*-PS block copolymers from the surface of montmorillonite and cartoon respresenting one "macromolecule" of MMT and bound BCP chains.

Block copolymers were synthesized via surface-initiated polymerization from MMT platelets by adapting established ARGET ATRP methods. Figure 1 shows the steps taken to prepare the BCP composites. First, sodium montmorillonite was ion-exchanged with a long alkyl chain surfactant that contains an initiator moiety for ATRP. The initiator-functionalized montmorillonite (MMT-SI) thus served as the initiator species for ARGET ATRP of *n*-butyl acrylate (nBA), which also included a copper catalyst species (copper(II) bromide, $CuBr_2$), a catalyst solubilizing ligand (tris(2-(dimethyl-amino)ethyl)amine, Me_6TREN), and a reducing agent (tin 2-ethylhexanoate, $Sn(EH)_2$) that allowed spent catalyst (Cu(II) state) to be recycled back to the active state (Cu(I)). After polymerization of the PnBA block, residual nBA monomer and anisole (solvent) were removed in vacuo because PnBA is a rubbery polymer at room temperature (T_g ~ -50 °C[22]) and does easily precipitate. Next, ARGET ATRP of styrene was conducted from the MMT-PnBA macroinitiator but without further addition of $CuBr_2$ or Me_6TREN, as these components remained

behind following removal of nBA and anisole. The resulting BCP composite material (MMT-PnBA-b-PS) was purified by precipitation because the glassy styrene block (T_g ~ 100 °C[23]) easily precipitates in methanol. Non-composite di- and tri-BCPs (PnBA-b-PS and PS-b-PnBA-b-PS) were also synthesized via ARGET ATRP, although with common small molecule single and double initiators.

Sample	PnBA		PnBA-*b*-PS		
MMT-PnBA-*b*-PS[a]	M_n (kDa)[b]	PDI[b]	M_n (kDa)[c]	PDI[b]	f_{PS}[c]
MBS-35	17.3	1.31	35.5	1.37	0.51
MBS-37	17.1	1.28	37.0	1.42	0.54
MBS-50	24.9	1.24	50.3	1.34	0.51
MBS-57	23.0	1.10	57.1	1.47	0.59
MBS-63	34.2	1.27	63.6	1.39	0.46
MBS-64	32.3	1.18	64.2	1.41	0.50
MBS-85	29.2	1.18	85.7	1.47	0.65
MBS-90	39.5	1.29	90.2	1.45	0.56
MBS-93	40.6	1.30	93.3	1.40	0.56
MBS-105	47.5	1.41	105.4	1.47	0.55
PnBA-*b*-PS	M_n (kDa)[d]	PDI[d]	M_n (kDa)[c]	PDI[d]	f_{PS}[c]
BS-38	20.1	1.26	38.7	1.07	0.48
BS-46	25.3	1.25	46.7	1.08	0.46
BS-55	25.6	1.24	55.5	1.11	0.54
BS-72	48.4	1.22	72.5	1.10	0.33
BS-103	62.1	1.20	103.3	1.12	0.40
PS-*b*-PnBA-*b*-PS	M_n (kDa)[d]	PDI[d]	M_n (kDa)[c]	PDI[d]	f_{PS}[c]
SBS-49	29.2	1.09	49.0	1.07	0.41
SBS-57	36.3	1.07	57.3	1.07	0.37
SBS-73	41.5	1.12	73.1	1.17	0.43
SBS-78	50.2	1.18	78.4	1.13	0.36
SBS-155	97.5	1.05	155.0	1.20	0.37

[a] Polymer chains characterized after cleaving from MMT. [b] Determined by GPC in DMF/LiBr. [c] Volume fraction PS. Determined by 1H NMR. M_n calculated from measured PS mole fraction. [d] Determined by GPC in THF.

Table 1. Properties of BCPs prepared by ARGET ATRP, using both surface-bound and single and di-functional small molecule initiators.

Table 1 shows the molecular weight (MW) and polydispersity index (PDI) properties of various synthesized BCPs. A wide range of molecular weights were targeted while maintaining the PS volume fraction near 0.5±0.1, targeting a lamellar BCP structure. The MW of triblock samples were targeted at double that of composite and diblock samples. Representative gel permeation chromatographs

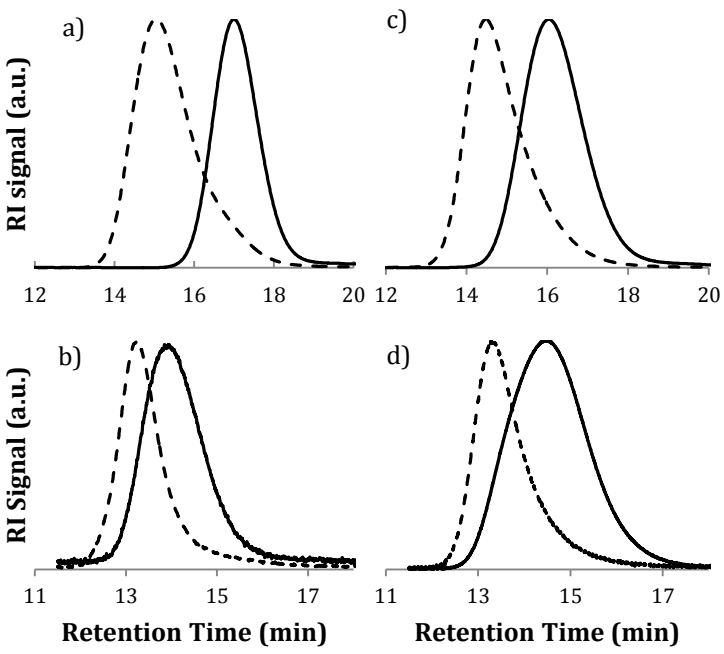

Figure 2. GPC traces of BCPs after the synthesis of each block. a and b) Samples MBS-57 and MBS-90, respectively. Samples run in DMF/LiBr after cleaving from MMT. c) Sample BS-55. Sample run in THF. d) Sample SBS-73. Sample run in THF. (—) PnBA block, (---) addition of PS block(s).

(GPC) of composite and non-composite BCPs are shown in Figure 2. The peak shift to lower retention time indicates growth of the composite samples, which typically have higher PDIs than non-composite samples, likely due to the differences in initiation between the two. In free initiator polymerizations, initiator molecules initiate polymerization almost immediately after addition of reducing agent to the polymerization solution because they exist free in solution and will easily come into contact with active catalyst. In a composite polymerization, however, many initiator moieties remain trapped in inter-gallery spaces between individual MMT platelets, where diffusion of the species necessary for ATRP to occur is reduced. Thus, initiation takes place over a longer period of time, during which platelets become intercalated with growing polymer chains, allowing for further infiltration of monomer, catalyst, and reducing agent. Furthermore, the addition of the PS block in composite samples results in higher PDIs compared to lower PDIs in non-composites, which is the expected result in BCP synthesis. As chains become longer, differences in length become less

pronounced. The higher PDIs probably result from propagating chain ends becoming buried in the growing polymer halo surrounding each MMT platelet and diffusion limitations within the halo[21c]. Some tailing at high retention times is evident in the PnBA-b-PS chromatograph of Figure 2a, sample MBS-57, indicating some PnBA chains may not have initiated PS blocks.

Composite BCPs were characterized by GPC using DMF with LiBr as an eluent as opposed to more commonly used THF. This is necessary because the quaternary ammonium end group of the surface initiator appears to interact with the GPC columns, delaying the elution of the polymer chains. DMF with LiBr, which is typically used when polyelectrolytes or polyimides are characterized by GPC[24], mitigates any charge interactions with the columns, allowing for adequate signal. When composite BCP samples were run in THF, a low signal peak was observed near the expected elution time, which proved difficult or impossible to analyze. Light scattering signals show evidence of large MW species eluting long after the small molecule peak. This seems to confirm a delayed elution phenomenon due to sample interactions with the columns. When run in DMF/LiBr, however, composite BCPs exhibited adequate signal at the expected elution time without signs of significant interactions between the columns and the polymer.

MMT-PnBA	Cu (ppm)[a]	Cu:I[b]	$Sn(EH)_2$:I[c]	t (hr)	Conv (%, exp.)[d]	Conv (%, theo.)[e]
MBS-64	400	0.1	2	3.7	92.6	99.5
MBS-105	250	0.1	2	3.3	89.6	91.9
MMT-PnBA-*b*-PS[f]						
MBS-64	240	0.1	0.1	21.3	49.1	73.0
MBS-105	150	0.1	0.1	48.0	66.0	85.6
PnBA (for diblock)						
BS-38	100	0.03	0.1	22.3	46.5	51.8
BS-103	100	0.05	0.1	22.8	87.4	96.6
PnBA-*b*-PS						
BS-38	120	0.03	0.1	50.5	82.9	68.8
BS-103	70	0.05	0.1	47.5	69.0	56.6
PnBA (for triblock)						
SBS-49	100	0.04	0.1	24.0	74.4	56.2
SBS-155	100	0.06	0.1	24.0	104.8	94.8
PS-*b*-PnBA-*b*-PS						
SBS-49	110	0.04	0.1	43.5	56.6	54.7
SBS-155	50	0.06	0.1	42.0	50.5	45.8

[a] Relative to monomer. [b] Molar ratio of Cu to initiator. [c] Molar ratio of $Sn(EH)_2$ to initiator. [d] Determined gravimetrically. [e] Determined based on molecular weight results. [f] $Sn(EH)_2$:I ratio reflects additional $Sn(EH)_2$ added to the polymerization solution upon initiation of PS block.

Table 2. Experimental conditions for ARGET ATRP of BCPs. Samples correspond to those in Table 1.

Table 2 shows the experimental conditions used in the synthesis of BCP samples. Most ARGET ATRP syntheses aim for 100 ppm of copper relative to monomer or lower. While non-composite BCPs were synthesized with copper amounts at or below this value, much higher concentrations of copper were necessary to facilitate control of the polymerization, again probably because of diffusion limitations during initiation and early stages of propagation. Similarly, higher concentrations of reducing agent were necessary for composite synthesis, with a $Sn(EH)_2$ to initiator ratio of 2 compared to the more typical 0.1 for initiators free in solution. The high concentration of reducing agent when synthesizing MMT-PnBA explains the rapid observed polymerization rate, with samples reaching over 90% conversion in less than 4 hours. This compares to about 24 hours required for PnBA for non-composite samples to reach at least 50% conversion, with lower MW samples (BS-38 and SBS-49) only reaching about 55% conversion and higher MW

samples (BS-103 and SBS-155) reaching about 95% conversion. Styrene polymerization is typically not very fast via ATRP, so most samples were allowed to react for almost two days or more, generally reaching conversions in the range 45-80%. Styrene ratios relative to initiator in the starting polymerization solution were adjusted based on expected conversions following numerous trial polymerizations.

3.2. Structural Characterization

Composite BCPs were examined by several techniques to ascertain their composition and structure. Figure 3 shows the results of thermogravimetric analysis (TGA) on samples representing various stages in the synthesis of the composite. Upon addition of the surface initiator to MMT, the total organic content of the clay increased by 22% after adjusting for inherent water content. Upon synthesis of the BCP, the total organic content increased to approximately 95±2% for all composite samples. The clay content of 5% or more compared to the total composition and approximately 10% or more compared to the MMT-PnBA is higher than is typically seen in more traditionally prepared clay composites (less than 5%)[9]. The high clay loading is expected to yield composites that exhibit superior material properties, such as fire retardancy, than tradition composites.

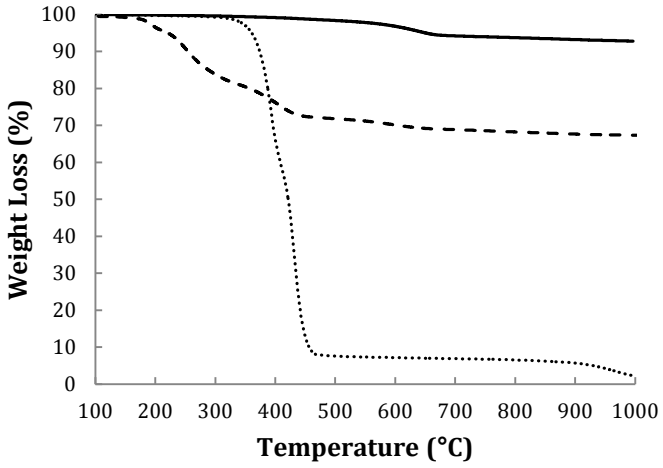

Figure 3. TGA profiles showing organic composition. (—) MMT from source, (---) MMT-SI, (···) MBS-90.

This consequence arises due to the nanoscale design of the polymer, in which individual chains are tethered to clay platelets, serving to both solubilize and anchor the filler in the bulk material.

Because degree of exfoliation has a known influence over property enhancement in composite materials, wide-angle x-ray scattering (WAXS) was conducted to gain an initial indication of the exfoliation of the MMT after synthesis. Figure 4 shows the results of WAXS measurements on samples at various synthetic stages.

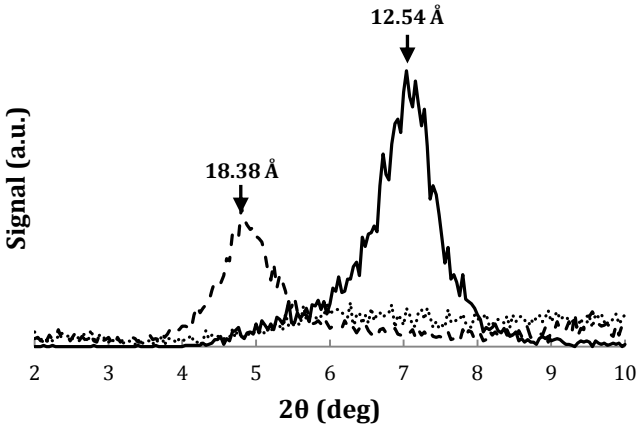

Figure 4. WAXS profiles with indicated scattering peaks and corresponding d-spacings. (—) MMT from source, (---) MMT-SI, (···) MBS-37.

Natural MMT has a well-characterized inter-gallery spacing (d-spacing) of 12.5 Å. This spacing increases to 18.4 Å upon addition of the surface initiator, denoting that the surface initiator has displaced the existing sodium cations and corroborating the TGA data. After synthesis of the BCP, no peak appears on the WAXS profile, which indicates that exfoliation of the MMT has occurred. It is not possible to determine the exact degree of exfoliation, however, and previous studies have demonstrated that WAXS data alone does not prove that complete exfoliation of the filler has occurred[9]. Subsequent microscopic analysis will more precisely reveal the degree of exfoliation.

To determine the structure of the BCP within the composite, small-angle x-ray scattering (SAXS) experiments were performed. SAXS profiles for composite and non-composite BCP samples are provided in Figure 5. Despite using a powerful synchrotron source for SAXS measurements, composite samples showed relatively low signal, even after background noise subtraction and adjustments. It is believed the presence of heavy atoms in the clay interfered with transmission of the x-ray beam by creating more opportunities for successive collision events. Still, several samples suggested a degree of ordering within the polymeric component of the composite. Samples MBS-85 and MBS-93 both exhibit scattering patterns indicative of lamellar structures[25], with higher-order scattering peaks at multiples of the primary scattering peak. Lower MW samples of the composite BCPs, such as MBS-37, showed very low signal, probably because of the slightly higher MMT content in these samples.

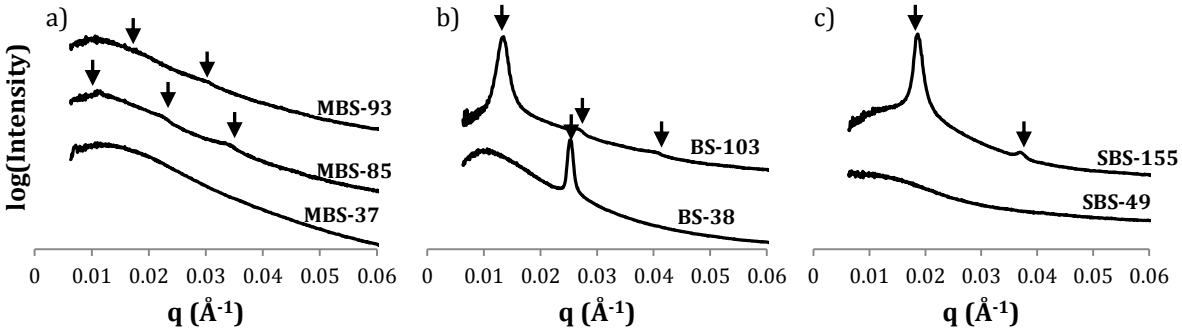

Figure 5. SAXS profiles after thermal annealing with indicated scattering peaks. a) MMT-PnBA-*b*-PS. b) PnBA-*b*-PS. c) PS-*b*-PnBA-*b*-PS. Profiles shifted vertically for clarity.

The SAXS profiles of the non-composite BCP samples were also examined. Figures 5b and 5c show profiles for di- and triblock samples respectively. The diblock samples exhibit lamellar ordering, even at the lowest MWs examined. Only the highest MW triblock samples showed any evidence of ordering. Flory-Huggins

theory explains this observation because tri-BCPs require higher MWs before ordering is observed[26]. These results indicate that by utilizing tethered filler materials, it is possible to create BCPs with pseudo-triblock architectures that still assemble at low MWs. Of course, it is logical to assume that BCP chains tethered to a two-dimensional nanoparticle such as MMT will be forced to self-assemble due to their severly restricted motion, regardless of their exact architecture. It would be interesting to explore the effects of other nanoparticle geometries on the ability to force BCP assembly at unexpected MWs.

BCP phase segregation can also be characterized by differential scanning calorimetry (DSC). Figure 6 shows DSC traces of composite BCP samples. Measurements were taken during the second heating cycle to reduce the influence of thermal history. Transitions at the T_gs of both PS and PnBA in all samples reveal that some degree of ordering has occurred, however, the sharpness of the transitions increases at higher MWs. The low and broad transitions of sample MBS-37 indicate a lower degree of self-assembly in that sample. Samples without ordering, such as the lower MW diblocks, show a DSC trace with one broad transition roughly between the T_gs of the individual blocks. The DSC data agrees with the SAXS data but suggests that a conclusion cannot

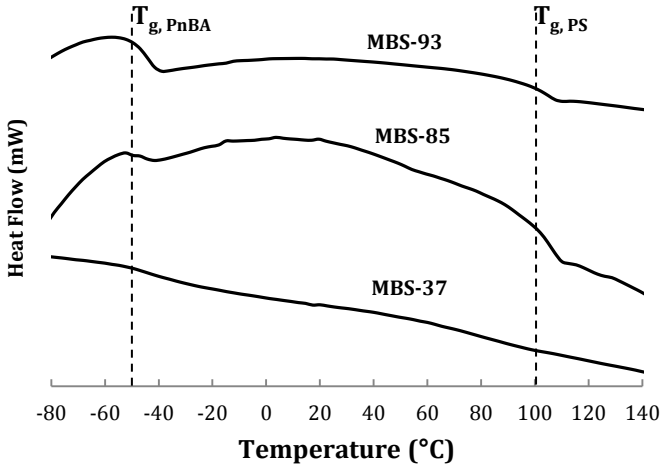

Figure 6. DSC traces of composite samples during second heating. Dashed lines indicate Tgs of PnBA and PS. Profiles shifted vertically for clarity.

be drawn about whether self-assembly has occurred in the lower MW composite samples merely from SAXS alone.

Transmission electron microscopy (TEM) provided the best opportunity to explore the structure of the composite. Figure 7 shows several transmission electron micrographs of composite BCP samples. The BCP exhibits a high degree of phase segregation with good contrast between the two polymer blocks without additional staining. It is possible to see non-exfoliated platelets as large elongated

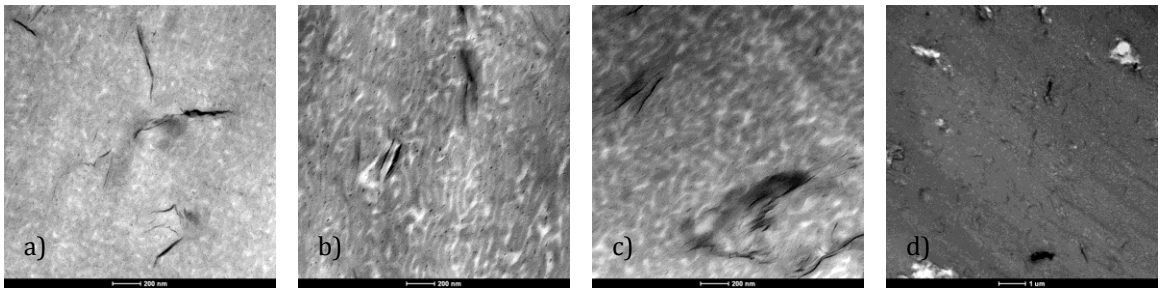

Figure 7. TEM micrographs of composite BCPs. a) MBS-85, b) MBS-90, c) and d) MBS-105.

shapes, however, as these shapes make up a small fraction of the total image area, it is assumed that most of the platelets are exfoliated. Individual platelets appear as very faint streaks or dots in the image and are difficult to completely resolve because their thickness (1 nm) is at the resolution limit of the instrument. The lamellar structure is evident but long range order is not present, except for some slight evidence around larger particulates. By utilizing other sample preparation methods, such as extrusion, it might be possible to achieve longer range order in bulk samples. It is apparent, however, that the majority of the platelets orient roughly parallel to one another. Other TEM images revealed stacks of semi-transparent platelets oriented in the plane that the section was cut. Figure 7d shows a TEM of sample MBS-105 at a lower magnification to reveal the difficulties

encountered when preparing TEM samples. Because the clay platelets are typically between 100 and 200 nm wide and TEM sections were cut at 60 nm wide, tears commonly occured during the sectioning process as platelets were ripped free by the cutting blade. Large tears can be seen in three of the corners of this image (7d).

During TEM imaging, all composite samples showed evidence of self-assembly, which was not entirely evident during SAXS and DSC measurements. Despite the difficulty in sample preparation, TEM is essential in revealing the structural features of the composites. In contrast, TEM was not particularly helpful in evaluating the non-composite BCPs. Those samples with confirmed phase separation by SAXS did not show good block contrast, even after staining sections with RuO_4. In the composites, the presence of MMT probably added to the contrast between the polymer blocks, allowing for direct imaging of the phases without staining.

3.3. Material Property Characterization

Only a preliminary characterization of the material properties of the composite materials and the respective non-composites was performed, but the initial data suggests several interesting features. Figure 8 shows rheological characterization of an assembled composite material and a non-assembled non-composite. Frequency sweeps of the composite (Figure 8a) revealed elastomeric behavior, with both the storage and loss (G' and G'') moduli roughly equaling each other. This effect was more pronounced in higher MW samples, coinciding with a higher degree of phase separation. The non-composite (Figure 8b) exhibited a higher loss than storage modulus at low frequencies and a storage to loss modulus

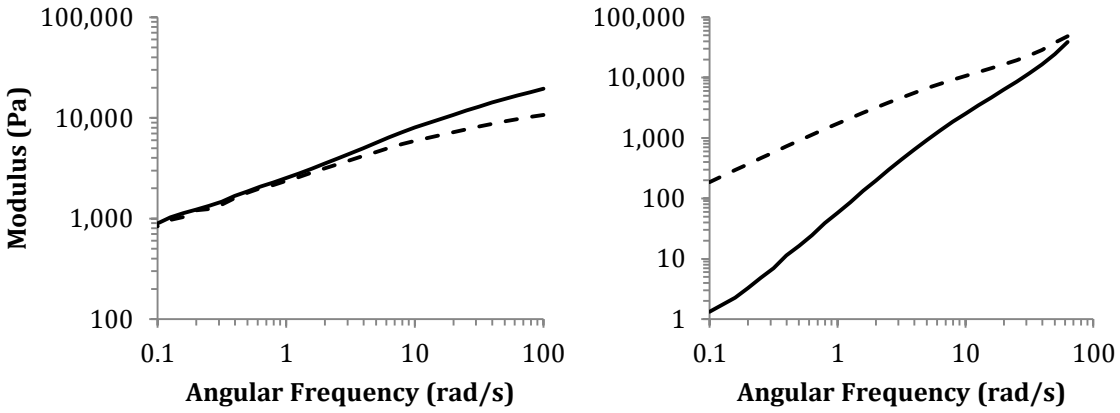

Figure 8. Rheological characterization of composite and non-composite BCPs. a) MBS-64. b) SBS-78. G' (—) and G'' (---).

slope ratio of 2:1, indicative of a non-ordered, homogeneous material. All composites exhibited somewhat elastomeric behavior. The moduli values are proportional to MW. These results confirm that the composite materials behave like thermoplastic elastomers, though more experiments are necessary to further quantify and validate these early experiments.

Initial dynamic mechanical analysis (DMA) experiments were performed on several of the composite samples. While the materials displayed high strength as evident by high initial modulus values, all tended to break relatively early after being stretched, indicating a high degree of brittleness. None of the composite samples were capable of being stretched without breakage to 10% elongation. A probable explanation for the observed brittleness is the inability of the polymer chains to fully entangle with one another. Because of surface tethering to the MMT platelets, the polymer chains are packed at high densities. While this packing might promote phase separation, the density of chains inhibits penetration of chains from neighboring platelets. Consequently, platelets and their surrounding polymer halos will merely pull apart from one another when tension is applied.

4. Conclusion

4.1. Summary of Findings

A library of MMT-PnBA-*b*-PS samples was successfully synthesized and characterized via several techniques to determine the structure of the composite. ARGET ATRP was used to control the architecture of the BCPs while simultaneously ensuring dispersion of MMT platelets.. The synthetic techniques developed are versatile in that they can be adapted to other BCPs and/or filler materials. Preliminary material property measurements indicate that the current materials may need to be slightly redesigned to improve upon brittleness issues.

4.2. Future Work

Future work should focus on examining the material properties of the composite materials. In additional to tensile and other mechanical testing, flame retardancy and barrier property measurements should be performed to further assess the utility of the materials in practical applications. To explore the issue of brittleness, two primary routes should be pursued. Blending the composite with homopolymers or block copolymers might improve entanglement of chains. Additionally, reducing the chain density on the surface of the MMT platelets would allow chains from adjacent platelets to more easily entangle. Chain density reduction can be achieved by replacing some of the initiator species with inactive species prior to polymerization. Both of these proposed solutions might ease the stresses applied under strain at boundaries between platelet “macromolecules”. Long-term research should explore additional block architectures and compositions,

including the inclusion of blocks with specific desirable traits, such as impermeability or selective transport.

5. Experimental Details

Materials

Sodium montmorillonite (Closite Na+) was generously supplied by Southern Clay Products, Inc. Styrene (Acros, 99%), *n*-butyl acrylate (nBA) (Acros, 99+%), and anisole (Acros, 99%) were stirred over basic alumina and calcium hydride to remove stabilizers and water. Tris(2-(dimethyl-amino)ethyl)amine (Me_6TREN) was synthesized according to a previously reported procedure[27]. 11′(N,N,N-trimethylammonium bromide)-undecyl-2-bromo-2-methyl propionate (SI) was synthesized according to a previously reported procedure[21b]. Ethyl α-bromoisobutyrate, dimethyl 2,6-dibromoheptanedioate, copper(II) bromide (Acros, 99+%), copper(II) chloride (Acros, 99%), tin(II) 2-ethylhexanoate ($Sn(EH)_2$) (Aldrich, 95%), lithium bromide (Acros, 99+%), tetrahydrofuran (THF) (Fisher), and N,N-dimethylformamide (DMF) (Aldrich, HPLC, >99.9%) were used as received.

Initiator-Functionalization of Montmorillonite (MMT-SI)

SI was ion-exchanged onto sodium montmorillonite (MMT). Five grams of MMT was dissolved in ~150 mL of DI water and sonicated for 15 minutes. Two grams of SI was dissolved in ~50 mL of DI water and added to the MMT slurry. The mixture was stirred vigorously overnight, after which the solids were isolated by filtration and dried in a vacuum oven at room temperature.

Synthesis of MMT-PnBA-*b*-PS

The effective molecular weight of the initiator species MMT-SI was determined by TGA. The SI molecular weight (380 g/mol) was divided by the organic fraction (~22%) to yield an effective molecular weight of 1727 g/mol. The

polymerization procedure was adapted from published ARGET ATRP procedures[5, 7]. Anisole, nBA, MMT-SI, $CuBr_2$ or $CuCl_2$, and Me_6TREN were added to a round-bottom flask, which was sealed with a septum and sparged with argon for 10 minutes. $Sn(EH)_2$ dissolved in anisole was added via syringe to initiate polymerization. Molar ratios of the above components for a representative polymerization were 200:1:0.1:1:2 for nBA, MMT-SI, $CuCl_2$, Me_6TREN, and $Sn(EH)_2$ respectively, with the nBA:MMT-SI ratio determining the desired molecular weight. Anisole was added at 30 wt%. The flask was placed in an oil bath at 60 °C. After a determined amount of time, the flask was immersed in liquid nitrogen for several seconds and exposed to atmosphere to stop the polymerization. Two samples were taken, one for determination of conversion gravimetrically and another for molecular weight characterization. The flask was then subjected to vacuum to remove solvent and unreacted nBA. Anisole and styrene were added to the flask to dissolve the MMT-PnBA. The flask was sealed and sparged with argon for 10 minutes. The addition of $Sn(EH)_2$ dissolved in anisole initiated the polymerization, which was allowed to proceed for a determined amount of time at 90 °C. Molar ratios of styrene, MMT-PnBA, and anisole for a representative polymerization were 400:1:0.1 respectively. Anisole was added at 50 wt%. The reaction was halted as before, and two samples were taken, one for conversion and one for molecular weight characterization. The composite was precipitated several times in excess methanol and freeze-dried from benzene.

Cleavage of BCP chains from MMT

PnBA and PnBA-*b*-PS chains were cleaved from MMT by stirring molecular weight characterization samples in THF with LiBr at room temperature for an hour. The solution was centrifuged and the supernatant dried to yield cleaved polymer.

Synthesis of Non-Composite BCPs

The polymerization procedure for non-composite di- and triblock copolymers was similar to that used to prepare composite BCPs. Ethyl α-bromoisobutyrate (EBiB) and dimethyl 2,6-dibromoheptanedioate were used as initiators for di- and triblock copolymers respectively. $CuBr_2$ was used at the catalyst. Molar ratios for a representative polymerization of PnBA are 400:1:0.04:0.4:0.1 for nBA, EBiB, $CuBr_2$, Me_6TREN, and $Sn(EH)_2$ respectively. Addition of the styrene block proceeded as with the composite synthesis. BCPs were precipitated several times in excess methanol and freeze-dried from benzene.

Measurements

Molecular weights and dispersities were determined by gel permeation chromatography (GPC). Composite BCPs were characterized with an Agilent 1200 Series isocratic pump and autosampler, Viscotek I-Series mixed bed medium and low MW columns, an Agilent 1100 Series refractive index detector, and DMF with 0.01M LiBr as the eluent at 35 °C and 1 mL min^{-1}. Poly(n-butyl acrylate) and polystyrene standards were used for calibration. Non-composite BCPs were characterized with a Viscotek GPCMax VE 2001 GPC solvent/sample module with a Viscotek Model 270 dual detector viscometer/light scattering detector, a Viscotek

VE 3580 refractive index detector, I-Series mixed bed medium and low MW columns, and THF as the eluent at 30 °C at 1 mL min^{-1}. Absolute characterization was conducted by Viscotek Triple Detect software combining light scattering, refractive index detection, and viscometry. All ^{1}H NMR spectra were recorded on a Varian Unity Plus 400 MHz instrument. Thermogravimetric analysis (TGA) was conducted on a Mettler-Toledo TGA/DSC 1 Thermogravimetric Analyzer using a ramp rate of 10 °C min^{-1} up to 1000 °C. Wide angle x-ray scattering (WAXS) measurements were conducted on a Philips X'Pert Powder x-ray diffractometer. Small angle x-ray scattering (SAXS) measurements were conducted at the National Synchrotron Light Source, Brookhaven National Laboratory on beamline x27c. The wavelength of the X-ray beam was 0.137 nm. The beam center was calibrated using silver behenate with the primary reflection peak at 1.076 nm^{-1}. Samples were annealed at 200 °C and cooled to room temperature before measurements were taken. Transmission electron micrographs were recorded on a FEI Technai Spirit TEM at an accelerating voltage of 80 kV. Ultrathin (~60 nm) sections were obtained by hot-pressing samples at 200 °C and sectioning blocks of material using a Leica Ultramicrotome at very cold temperatures (~ -60 °C), below the T_g of the PnBA block. Rheological measurements were taken on a TA Instruments AR-2000EX rheometer. Dynamical mechanical analysis (DMA) measurements were recorded on a TA Instruments Q800 DMA.

References

1. Wang, J. S.; Matyjaszewski, K., Controlled Living Radical Polymerization - Halogen Atom-Transfer Radical Polymerization Promoted by a Cu(I)Cu(II) Redox Process. *Macromolecules* **1995,** *28* (23), 7901-7910.
2. Wang, J. L.; Grimaud, T.; Matyjaszewski, K., Kinetic study of the homogeneous atom transfer radical polymerization of methyl methacrylate. *Macromolecules* **1997,** *30* (21), 6507-6512.
3. Davis, K. A.; Matyjaszewski, K., Atom transfer radical polymerization of tert-butyl acrylate and preparation of block copolymers. *Macromolecules* **2000,** *33* (11), 4039-4047.
4. Matyjaszewski, K.; Wang, J. L.; Grimaud, T.; Shipp, D. A., Controlled/"living" atom transfer radical polymerization of methyl methacrylate using various initiation systems. *Macromolecules* **1998,** *31* (5), 1527-1534.
5. (a) Matyjaszewski, K.; Jakubowski, W.; Min, K.; Tang, W.; Huang, J. Y.; Braunecker, W. A.; Tsarevsky, N. V., Diminishing catalyst concentration in atom transfer radical polymerization with reducing agents. *Proc. Natl. Acad. Sci. U. S. A.* **2006,** *103* (42), 15309-15314; (b) Jakubowski, W.; Min, K.; Matyjaszewski, K., Activators regenerated by electron transfer for atom transfer radical polymerization of styrene. *Macromolecules* **2006,** *39* (1), 39-45.
6. Xia, J. H.; Matyjaszewski, K., Controlled/"living" radical polymerization. Atom transfer radical polymerization using multidentate amine ligands. *Macromolecules* **1997,** *30* (25), 7697-7700.

7. Jakubowski, W.; Matyjaszewski, K., Activators Regenerated by Electron Transfer for Atom-Transfer Radical Polymerization of (Meth)acrylates and Related Block Copolymers. *Angewandte Chemie International Edition* **2006,** *45* (27), 4482-4486.

8. Matyjaszewski, K.; Dong, H. C.; Jakubowski, W.; Pietrasik, J.; Kusumo, A., Grafting from surfaces for "Everyone": ARGET ATRP in the presence of air. *Langmuir* **2007,** *23* (8), 4528-4531.

9. Paul, D. R.; Robeson, L. M., Polymer nanotechnology: Nanocomposites. *Polymer* **2008,** *49* (15), 3187-3204.

10. LeBaron, P. C.; Wang, Z.; Pinnavaia, T. J., Polymer-layered silicate nanocomposites: an overview. *Applied Clay Science* **1999,** *15* (1), 11-29.

11. Krishnamoorti, R.; Vaia, R. A., Polymer nanocomposites. *Journal of Polymer Science Part B-Polymer Physics* **2007,** *45* (24), 3252-3256.

12. Vaia, R. A.; Maguire, J. F., Polymer nanocomposites with prescribed morphology: Going beyond nanoparticle-filled polymers. *Chemistry of Materials* **2007,** *19* (11), 2736-2751.

13. Fredrickson, G. H.; Bicerano, J., Barrier properties of oriented disk composites. *J. Chem. Phys.* **1999,** *110* (4), 2181-2188.

14. Fertig, R. S.; Garnich, M. R., Influence of constituent properties and microstructural parameters on the tensile modulus of a polymer/clay nanocomposite. *Compos. Sci. Technol.* **2004,** *64* (16), 2577-2588.

15. Bockstaller, M. R.; Mickiewicz, R. A.; Thomas, E. L., Block copolymer nanocomposites: Perspectives for tailored functional materials. *Adv. Mater.* **2005,** *17* (11), 1331-1349.

16. (a) Stamatialis, D. F.; Stafie, N.; Buadu, K.; Hempenius, M.; Wessling, M., Observations on the permeation performance of solvent resistant nanofiltration membranes. *J. Membr. Sci.* **2006,** *279* (1-2), 424-433; (b) Chen, X.; Zhao, D. Y.; An, Y. L.; Zhang, Y.; Cheng, J.; Wang, B. L.; Shi, L. Q., Formation and catalytic activity of spherical composites with surfaces coated with gold nanoparticles. *J. Colloid Interface Sci.* **2008,** *322* (2), 414-420.

17. Mistark, P. A.; Park, S.; Yalcin, S. E.; Lee, D. H.; Yavuzcetin, O.; Tuominen, M. T.; Russell, T. P.; Achermann, M., Block-Copolymer-Based Plasmonic Nanostructures. *Acs Nano* **2009,** *3* (12), 3987-3992.

18. Arico, A. S.; Bruce, P.; Scrosati, B.; Tarascon, J. M.; Van Schalkwijk, W., Nanostructured materials for advanced energy conversion and storage devices. *Nat. Mater.* **2005,** *4* (5), 366-377.

19. Balazs, A. C.; Emrick, T.; Russell, T. P., Nanoparticle polymer composites: Where two small worlds meet. *Science* **2006,** *314* (5802), 1107-1110.

20. Advincula, R., Polymer brushes by anionic and cationic Surface-Initiated Polymerization (SIP). In *Surface-Initiated Polymerization I*, Springer-Verlag Berlin: Berlin, 2006; Vol. 197, pp 107-136.

21. (a) Bottcher, H.; Hallensleben, M. L.; Nuss, S.; Wurm, H.; Bauer, J.; Behrens, P., Organic/inorganic hybrids by 'living'/controlled ATRP grafting from layered silicates. *Journal of Materials Chemistry* **2002,** *12* (5), 1351-1354; (b) Zhao, H.

Y.; Shipp, D. A., Preparation of poly(styrene-block-butyl acrylate) block copolymer-silicate nanocomposites. *Chemistry of Materials* **2003,** *15* (14), 2693-2695; (c) Behling, R. E.; Williams, B. A.; Staade, B. L.; Wolf, L. M.; Cochran, E. W., Influence of Graft Density on Kinetics of Surface-Initiated ATRP of Polystyrene from Montmorillonite. *Macromolecules* **2009,** *42* (6), 1867-1872.

22. Fioretto, D.; Livi, A.; Rolla, P. A.; Socino, G.; Verdini, L., THE DYNAMICS OF POLY(N-BUTYL ACRYLATE) ABOVE THE GLASS-TRANSITION. *J. Phys.-Condes. Matter* **1994,** *6* (28), 5295-5302.

23. Penwell, R. C.; Porter, R. S., VISCOSITY OF POLYSTYRENE NEAR GLASS TRANSITION. *J. Appl. Polym. Sci.* **1969,** *13* (11), 2427-&.

24. Hann, N. D., Effects of lithium bromide on the gel-permeation chromatography of polyester-based polyurethanes in dimethylformamide. *Journal of Polymer Science: Polymer Chemistry Edition* **1977,** *15* (6), 1331-1339.

25. Bates, F. S.; Fredrickson, G. H., Block Copolymer Thermodynamics: Theory and Experiment. *Annu. Rev. Phys. Chem.* **1990,** *41* (1), 525-557.

26. Mai, S. M.; Mingvanish, W.; Turner, S. C.; Chaibundit, C.; Fairclough, J. P. A.; Heatley, F.; Matsen, M. W.; Ryan, A. J.; Booth, C., Microphase-separation behavior of triblock copolymer melts. Comparison with diblock copolymer melts. *Macromolecules* **2000,** *33* (14), 5124-5130.

27. Fu, G. D.; Xu, L. Q.; Yao, F., Smart Nanofibers with a Photoresponsive Surface for Controlled Release. *Acs Applied Materials & Interfaces* **2009,** *1* (11), 2424-2427.